Applied Catalysis A, General 706 (2025) 120467

Contents lists available at ScienceDirect

Applied Catalysis A, General

journal homepage: www.elsevier.com/locate/apcata

Dehydration of xylose to furfural catalyzed by highly stable W-Nb-O mixed oxides Bronzes

Francisco Cernicharo-Toledo [a], Agustín de Arriba [a], Jesús López-Sánchez [b], José M. López-Nieto [a], Marcelo E. Domine [a,*]

[a] Instituto de Tecnología Química (UPV–CSIC), Universitat Politécnica de València, Consejo Superior de Investigaciones Científicas, Avda. Los Naranjos S/N, Valencia 46022, Spain

[b] Departamento de Electrocerámica, Instituto de Cerámica y Vidrio, Consejo Superior de Investigaciones Científicas, Calle Kelsen 5, Madrid 28049, Spain

ARTICLE INFO

Keywords:
Xylose dehydration
Furfural synthesis
Acid catalyst
Niobium doped tungsten oxides

ABSTRACT

In this work, the dehydration reaction of xylose (a representative C5 sugar) to furfural has been studied over W-Nb-O mixed oxides presenting hexagonal or pseudo-crystalline Bronze-type structure with controlled textural and acid properties, and also high stability under reaction conditions. Thus, a series of W-Nb-O metal oxides with different W/Nb ratios have been prepared hydrothermally, characterized by several physicochemical techniques and tested in autoclave-type reactors in liquid phase. Their influence on the catalytic activity has been assessed by tuning the Brønsted/Lewis acid properties of W-Nb-O materials. Interestingly, optimal catalytic results for the dehydration of xylose to furfural in monophasic system (water/ethanol mixture) were achieved for $W_{0.20}Nb_{0.80}O_x$ catalyst, with a furfural selectivity comparable to that of sulfuric acid industrial catalyst. Furfural productivity (0.683 $g_{Fur} \cdot g_{Cat}^{-1} \cdot h^{-1}$) attained with this W-Nb-O catalyst was higher than that calculated for most relevant and recently reported solid acid catalysts working in both mono- and bi-phasic systems, respectively. Catalytic activity of W-Nb-O material remained practically unchanged after three consecutive reuses, while structure and chemical composition of material were maintained unaltered either after three catalytic cycles or after 14 days experiment carried out under optimal reaction conditions. Reactivity results have been explained on the combination of both Brønsted and Lewis acid sites as a result of the different incorporation of niobium into the bronze structure.

1. Introduction

Biomass is a general term for all organic materials derived from plant and animal waste, such as wood from natural forests, waste from agricultural and forestry processes, and industrial, human or animal wastes [1]. Furthermore, nowadays, the decrease of fossil resources (i.e., gas, carbon and petroleum), combined with an increasing energy and fuels demand by emerging economies, and political and environmental concerns about carbon oxide emissions, make it imperative to develop economical and energy efficient processes for the sustainable production of renewable fuels and chemicals, with low-to-none carbon footprint. In this sense, lignocellulosic or plant biomass stands out as the only renewable source of carbon on Earth [2,3]; moreover, biofuels (this meaning fuels derived from plant biomass) are the most available and sustainable alternative for the production of liquid fuels, since greenhouse emissions associated with their production are far lower than fossil-based ones, even achieving net zero emissions if efficient production methods are used [4–6].

Among the different types of biomasses, lignocellulosic biomass is the cheapest and most abundant of them, composed of three major components, cellulose, hemicellulose and lignin, with small amounts of extractives and ash. Cellulose macromolecules regularly gather to form tough microfibers that function as the skeleton material of the cell wall, and the inner space is packed with amorphous hemicellulose and lignin linking material. Cellulose (30–50 wt% of biomass), sugar polymer composed only by glucose, connects with hemicellulose or lignin molecules mainly through hydrogen bonds, while the connections between hemicellulose and lignin include both hydrogen and covalent bonds (see Figure S1, Supporting Information). On the other hand, hemicellulose (20–40 wt% of biomass) is a sugar polymer containing five-carbon (usually xylose and arabinose) and six-carbon atoms (galactose, glucose and mannose). Interestingly, the most abundant building block

* Corresponding author.
E-mail address: mdomine@itq.upv.es (M.E. Domine).

https://doi.org/10.1016/j.apcata.2025.120467
Received 10 April 2025; Received in revised form 25 June 2025; Accepted 27 July 2025
Available online 28 July 2025

of hemicellulose is xylan (a xylose polymer linked at positions 1 and 4), useful for the production of fine chemicals and some precursors/additives for fuels.

Therefore, lignocellulosic raw material can be converted into fuels and chemicals by different primary routes. In this sense, syn-gas production via gasification, bio-oil production by pyrolysis or liquefaction, and specific hydrolysis of biomass to produce sugar monomer units are typically studied [7]. After these primary treatments, a wide variety of products of interest can be obtained from biomass, including bio-compounds or platform molecules such as furfural, 5-hydroxymethylfurfural (5-HMF), levulinic acid, γ-valerolactone, and others [8]. In this way, furfural is an important raw material useful as building-block for furan-based chemicals and a major chemical for the production of biofuels and biochemicals, such as methylfuran [9,10], furfuryl alcohol [8,9], tetrahydrofurfuryl alcohol [11,12], tetrahydrofuran [10,12], dihydropyran [10,12,13], and furoic acid [10,14], among others.

Furfural current industrial production occurs through the selective dehydration of C5 sugars present in the hemicellulosic fraction by employing acid catalysts, sulfuric acid under homogeneous conditions being the most commonly used catalyst [19–21]. China (the world's largest exporter of furfural) adopted the Quaker Oats methodology to develop its own process (West pro-modified Huaxia Technology) starting from corn cobs with 3–4 wt% of sulfuric acid as catalyst. Apart from this process, there are others industrially employed such as Suprayield, S-SC [10], CIMV or MTC [1], for instance, always using H_2SO_4 as homogeneous catalyst and with maximum furfural yields ranging between 50 % and 70 %. In fact, hemicellulose (mainly compose by xylan) degradation into pentosan and its further depolymerization to pentoses (i.e., xylose) needs to be carried out under acid conditions, usually performed at relatively high temperatures (>140 ºC). Hence, selectivity to furfural under these reaction conditions is set at ca.70 %, although higher values (up to 80 %) have been reported by continuous extraction with organic solvents [15,16] (i.e., toluene, MIBK) or supercritical CO_2 [17], and even by new reactor engineering developments enhancing mineral acid and sugars interactions/contacts and/or furfural extraction by organic solvents [18–22]. Nevertheless, due to the hazardous properties of mineral or liquid acids such as sulfuric acid and the well-known drawbacks of homogeneous catalytic processes, there has been a great effort to replace toxic liquid acid catalyst by more environmentally friendly solid acid catalysts [23–25].

In the last years, the use of solid acid catalysts presenting both Brønsted and Lewis acid sites has been explored. Among others, acidic ionic exchange resins (i.e. Amberlyst 70) [26], silica-alumina based materials [27], microporous materials like zeolites (i.e. H-ZSM-5, H-SAPO-34) [28,29], mesoporous niobium oxide [30], transition metal oxides [31], heteropolyacids (HPAs) [32] and carbon-based sulphonated materials [33], have been used as catalysts for furfural production from different C5 enriched streams. Particularly, small pore H-SAPO-34 [34] and medium pore H-ZSM-5 [35] zeolites have been used as solid catalysts for furfural synthesis in both monophasic (water/γ-valerolactone) and biphasic (water/toluene) systems, respectively. In the former case, furfural yields close to 40 % were achieved, while better results (82.4 % yield) were *a priori* reported for H-ZSM-5 catalyst, but the way or method for determining the latest results are not well described or specified by the authors. Different Nb-based catalytic systems have also been studied for sugars dehydration to furfural. In this sense, niobium-containing catalysts, such as Nb-oxide supported on MCM-41 (MCM-Nb16) [36] and Nb-incorporate on mesoporous silicates (H-AM11) [37] have been used with water/toluene solvent system yielding 60 % and 54 % of furfural, respectively. These results are slightly better than 50 % furfural yield achieved with Nb_2O_5 by using the same water/toluene biphasic system [30], although better results (68 % furfural yield) have been reached with Nb_2O_5-type catalyst using water/CPME monophasic solvent system [38].

In general, the use of solid catalysts holds promising results to reduce associated production costs by eliminating corrosiveness of the reaction media and minimizing separation/neutralization costs. Regretfully, up to now, catalyst deactivation mostly due to carbon and/or heavy polymeric compounds (namely humins) deposition onto the active sites of the catalysts remains an important technological challenge [39–41].

In light of the above-mentioned, the replacement at industrial scale of mineral sulfuric acid by using more sustainable solid acid catalysts that maximize furfural production avoiding the formation of byproducts is of special interest. For this purpose, the development of heterogeneous catalysts with controlled acid properties, including the adequate combination of Brønsted and Lewis acid sites, and high resistance to deactivation under furfural synthesis conditions even in the presence of huge amount of water is required. In this regard, hydrothermally synthesized W-Nb-O mixed oxides with either hexagonal tungsten bronze (HTB) or pseudo-crystalline structure have emerged as robust and selective catalysts capable to conduce different acid-mediated catalytic reactions, such as selective dehydration of glycerol and consecutive condensations of light oxygenated organic compounds in aqueous media [42,43], and more recently, the N-alkylation of aniline with benzyl alcohol [44]. In this work, it is presented the synthesis and detailed characterization of W-Nb-O based materials, with different chemical composition, applied in the selective dehydration of xylose (selected as representative molecule of C5 sugars fraction) for the production of furfural in aqueous media under moderate reaction conditions. The tuning of the acid properties of W-Nb-O materials through their chemical composition control from the synthesis, and their influence on the catalytic activity observed will be assessed by adequate characterization of the solids. Optimization of reaction conditions to maximize furfural yield, the possibility of using mono- or bi-phasic reaction systems, as well as the stability and recyclability of the solid catalyst under reaction conditions will be studied. Finally, main results here reported for this robust W-Nb-O catalyst, mainly considering stability and recyclability, carbon balances in reactions, and furfural productivity (calculated as $g_{Fur} \cdot g_{Cat}^{-1} \cdot h^{-1}$), were compared with these data reported or calculated for most relevant and recently reported solid acid catalysts working in both mono- and bi-phasic solvent systems; thus, emphasizing the significance and robustness of the results here discussed. This novel solid catalyst development could be helpful for upscaling of furfural production through an heterogenous catalytic system, thus making furfural more accessible for further transformations towards high-added value industrial products [45].

2. Experimental procedure

2.1. Materials and reagents

Xylose (Sigma-Aldrich, 99.0 %), xylulose (Sigma-Aldrich, 95 %), furfural (Sigma-Aldrich, 99.0 %), L-pyroglutamic acid (Fluka, 99.0 %), mQ water (milliQ, Millipore), ethanol (Scharlab, 96.0 %), toluene (Scharlab 99.9 %), ammonium metatungstate hydrate (Sigma-Aldrich, 85.0 %), niobium oxalate (Sigma-Aldrich, 99.9 %), sulfuric acid (Sigma-Aldrich, 96 %) were used without any treatment.

2.2. Catalyst preparation

W-Nb-O mixed metal oxides, with Nb/(W+Nb) molar ratios ranging from 0 to 1, were prepared by hydrothermal synthesis from aqueous solutions (pH = 1, with HCl 3 M) of the metallic precursors, i.e., ammonium metatungstate hydrate and niobium oxalate, following previously reported methods [42]. Synthesis gels were transferred to Teflon-lined stainless-steel autoclaves and heated at 175 ºC for 48 h. Subsequently, formed solids were thermally activated at 550 ºC for 2 h under N_2 stream. Samples have been named as $\mathbf{W_yNb_zO_x}$, where y and z represent the molar percentage of tungsten and niobium, respectively, in the synthesis gel, considering each catalyst derive from pure WO_3 oxide.

For comparison, pure tungsten oxide and pure niobium oxide have

been also prepared by hydrothermal synthesis. Pure tungsten oxide (named as $\mathbf{W_{1.0}O_x}$) pure niobium oxide (named as $\mathbf{Nb_{1.0}Ox}$) were activated at 400 ºC/2h [42] and 550 ºC/2 h [46], respectively, under N_2 stream.

In addition, WO_3 (Sigma-Aldrich, 99.9 %), Nb_2O_5 (Sigma-Aldrich, 99.9 %), Amberlyst-15® ionic-exchange polymeric resin (Sigma-Aldrich), H-Beta with Si/Al molar ratio of 38/1 (Zeolyst), and H-USY with Si/Al molar ratio of 30/1 (Zeolyst) commercially available materials were used as acid solid catalysts for comparative purposes.

2.3. Catalyst characterization

Powder X-ray diffraction patterns (XRD) were collected using a Panalytical X´Pert diffractometer equipped with a graphite monochromator operating at 40 kV and 30 mA, employing Ni-filtered CuKα radiation (λ= 0.1542 nm). Specific surface areas were determined from N_2 adsorption isotherms at −190 ºC, using the BET method, in a Micromeritics ASAP 2000 instrument. Samples were previously degassed under vacuum at 250 ºC before adsorption. Thermogravimetric studies (TG) were carried out in a Mettler Toledo TGA/SDTA 851 apparatus. Samples were heated at 10 ºC min^{-1} from room temperature up to 800 ºC.

FTIR spectra of both as made and thermally activated samples were recorded using a Nicolet 205xB spectrophotometer with a spectral resolution of 1 cm^{-1} in the 400–4000 cm^{-1} region at room temperature (128 accumulations per scan). Previously, samples were milled and mixed with spectroscopic grade KBr and subsequently pressed into pellets.

IR spectra of adsorbed NH_3 were recorded in a Thermo "is50" spectrometer using a DTGS detector, acquired at 4 cm^{-1} resolution, with homemade glass IR cell that allows in situ treatments. For each experiment, a previous activation at 250 ºC for 1.5 h was considered, followed by evacuation at 10^{-4} mbar at said temperature for 1 h. Afterwards, samples were cooled down to room temperature and NH_3 was dosed at increasing pressure (0.4–25 mbar) until saturation, followed by evacuation. The temperature was then increased to 100 ºC under vacuum. IR spectra were recorded after each dosage and after each evacuation temperature.

Ammonia temperature programmed desorption (NH_3-TPD) experiments were performed in a Micromeritics TPD/2900 equipment. Then, samples (ca. 100 mg) were heated at 300 ºC for 1 h under argon flow to be subsequently cooled down to 100 ºC and saturated with ammonia. Afterwards, solids were kept under inert gas flow (100 ºC/15 min) to eliminate physically adsorbed NH_3. TPD analyses were carried out in the 100–500 ºC temperature range (heating rate of 10 ºC min^{-1}) with desorbed ammonia being analyzed by both mass spectroscopy and a thermal conductivity detector (TCD) analyzer.

The vibrational properties were analyzed using a confocal Raman microscope Witec ALPHA 300RA. This instrument is equipped with a ND:YAG laser light source of 532 nm wavelength and p-polarization aligned parallel to the x-axis. The microscope offers an optical resolution of ~200 nm laterally and ~500 nm vertically. Under optimal measurement conditions, the spectral resolution is 0.02 cm^{-1} . Raman spectra were recorded within the spectral range of 65–3850 cm^{-1} , using a 600 g $\cdot mm^{-1}$ grating. Measurements were conducted at room temperature, employing an objective lens with a numerical aperture of 0.95. An output laser power of 1 mW was used to prevent overheating effects and the formation of undesirable phases [47]. Data were processed using the Witec Project Plus software (version 2.08). Subsequently, average Raman spectra and Raman intensity images in the XY plane of the W-Nb-O mixed oxides are calculated from representative areas.

The crystal morphology was studied by both Scanning (SEM) and Transmission (TEM) Electron Microscopy. In the case of SEM analyses, micrographs were acquired in a ZEISS ULTRA 55 Field Emission Microscope, working at a voltage of 2 kV. Average chemical composition was also determined by energy-dispersive X-ray spectroscopy (XEDS), with an acquisition time for each spectrum of 120 s, by using an Oxford LINK ISIS detector attached to the microscope. Conversely, HR-TEM micrographs were taken in a Jeol JEM-2100F microscope with a field emission gun operated at 200 kV, equipped with a high-angle annular dark field (HAADF) detector. Samples were suspended in CH_2Cl_2 and then drop-cast on carbon-coated Ni grids (3 mm diameter) subsequently air-dried. Image analyses were performed with Gatan Digital Micrograph software. Measures took place at the Microscopy Service of the Polytechnic University of Valencia (UPV).

X-ray photoelectron spectroscopy (XPS) measurements were performed on a SPECS spectrometer at ultra-high vacuum (10^{-9} mbar), equipped with a Phoibos 150 MCD-9 detector, and using a non-monochromatic Al Kα X-ray source (1486.6 eV). Analyzer pass and X-ray power were 30 eV and 100 W, respectively. For the data treatment, CasaXPS software was employed, referencing all signals to the C *1 s* signal at 284.5 eV.

Finally, chemical analyses of selected fresh and reused samples were performed by inductively coupled plasma atomic emission spectrometry (ICP-AES) using a Varian 715-ES spectrophotometer calibrated with solutions of the elements of interest. Moreover, reused samples were also analyzed by Elemental Analysis (EA) in a Fisons EA1108CHN-S equipment to determine the amount of Carbon (C wt%) deposited on the solids after reaction.

2.4. Catalytic tests

Catalytic tests were performed in a 12 mL Teflon-lined stainless steel autoclave reactor equipped with a magnetic stirrer, temperature and pressure controllers, and a valve for liquid/gaseous sample injection and/or extraction. Typically, 10 wt% xylose in water or in H_2O/alcohol mixtures were poured into a Teflon container inside the reactor along with ca. 160 mg of catalyst, and it was hermetically closed. The xylose dehydration reaction was performed at 160 ºC with continuous stirring (1000 rpm) under autogenous pressure during 3 h. Liquid aliquots (≈100 μL) were taken at different time intervals, filtered off, cooled to room temperature and diluted in a 0.25 wt% L-pyroglutamic acid aqueous solution before HPLC analyses using an Agilent 1200 chromatograph equipped with RI detector and a Bio-Rad Aminex HPX-87H column, with 5 mM H_2SO_4 as mobile phase at 60 ºC.

Conversion was calculated through Eq. (1) by comparing the amount of xylose added at the beginning of the reaction with that determined by the HPLC measurement of the final mixture at the end of reaction, where n^0_{xylose} corresponds to the initial moles of xylose and n^f_{xylose} corresponds to the final moles of xylose:

$$C_{Xylose}(\text{mol\%}) = \frac{n^0_{xylose} - n^f_{xylose}}{n^0_{xylose}} \times 100 \quad (1)$$

Selectivity for each one of the different products detected in the final mixture was calculated through Eq. (2) by considering the amount of xylose converted as a function of the total amount of products in the liquid fraction, where and n^0_{xylose} corresponds to the initial moles of xylose and $n^f_{product}$ correspond to the final moles of products (e.g. furfural):

$$S_{product}(\text{mol\%}) = \frac{n^f_{product}}{n^0_{xylose} - n^f_{xylose}} \times 100 \quad (2)$$

The yield was defined as the quotient between the amount of desired product (i.e. furfural) and the amount of xylose present in the initial mixture, where and n^0_{xylose} corresponds to the initial moles of xylose and $n^f_{product}$ correspond to the final moles of products (e.g. furfural):

$$Y_{Desired\ product}(\text{mol\%}) = \frac{n^f_{product}}{n^0_{xylose}} \times 100 \quad (3)$$

3. Results and discussion

3.1. Structural, textural and physicochemical characterization of W-Nb-O mixed oxides

Fig. 1 and Figure S2 (in Supporting Information) show XRD patterns of heat-treated catalysts, while a summary of the main physicochemical properties of the catalysts can be observed in Table 1. The XRD patterns of pure tungsten oxide can be related to hexagonal tungsten oxide bronze (HTB, *h*-WO_3) structure, with diffraction peaks at 2θ = 14.0; 23.2; 28.1 and 36.9º (JCPDS: 85–2460) [48] whereas the XRD patterns of pure niobium oxide can be related to a pseudo-hexagonal niobium oxide (JCPDS: 28–0317), with peaks at 2θ = 22.6 and 46.4º, related to (001) and (002) planes, and broad peaks at 2θ = 25.9, 36.6 and 56.1º, respectively [49].

W-Nb-O mixed oxides with Nb/(W+Nb) molar ratio lower than 0.30 maintain hexagonal tungsten oxide bronze (HTB) structure, with main diffraction peaks appearing at 2θ = 14.0; 23.2; 28.1 and 36.9º (JCPDS: 33–1387), respectively [50]. In addition, it is well known that pure hexagonal tungsten oxide is stable up to 450 ºC [50]. However, Nb-doped tungsten oxide catalysts with Nb/(W+Nb) molar ratio lower than 0.30 are able to maintain the HTB structure with heat-treatment up to 550 ºC.

Conversely, for W-Nb-O materials with Nb/(W+Nb) molar ratio higher than 0.30, it is only observed the presence of a pseudo-crystalline phase, mainly ordered in the *c* axis, with an intense X-ray diffraction peaks at 2θ = 22.7 and 46.2º [51]. In addition, these samples shown additional broad peaks at 2θ = 26.1; 35.0; 49.6; 54.3 and 55.8 º (for samples with Nb/(W+Nb) ratio in the range of 0.30–0.55) or at 2θ = 26.9; 36.5; 46.5; 51.0; and 55.6º (for samples with Nb/(W+Nb) ratio of 0.60–0.90), respectively.

On the other hand, these differences in composition and/or crystallinity also seem to have notable influences in the acid characteristics of these catalysts. Then, Fig. 2A displays the NH_3-TPD results for selected samples, while the calculated results of ammonia adsorption are depicted in Table 1.

As expected, the progressive incorporation of Nb^{5+} species into the W-based material gives rise to a change in the acid characteristics of the samples. Then, ammonia desorption maxima observed in Fig. 2A profiles for the different catalysts show a shift from ca. 300 ºC, in the $\mathbf{W_{1.0}O_x}$ sample (related to Brønsted acid sites) to ca. 200 ºC (related to Lewis acid sites) in the catalysts with the highest Nb content (see Figs. 2A-e and 2A-f) [51]. These results suggest that the strength of the acid sites in materials with higher Nb-contents is lower than those presenting HTB structure (i.e., samples with Nb-content lower than 30 %). Nevertheless,

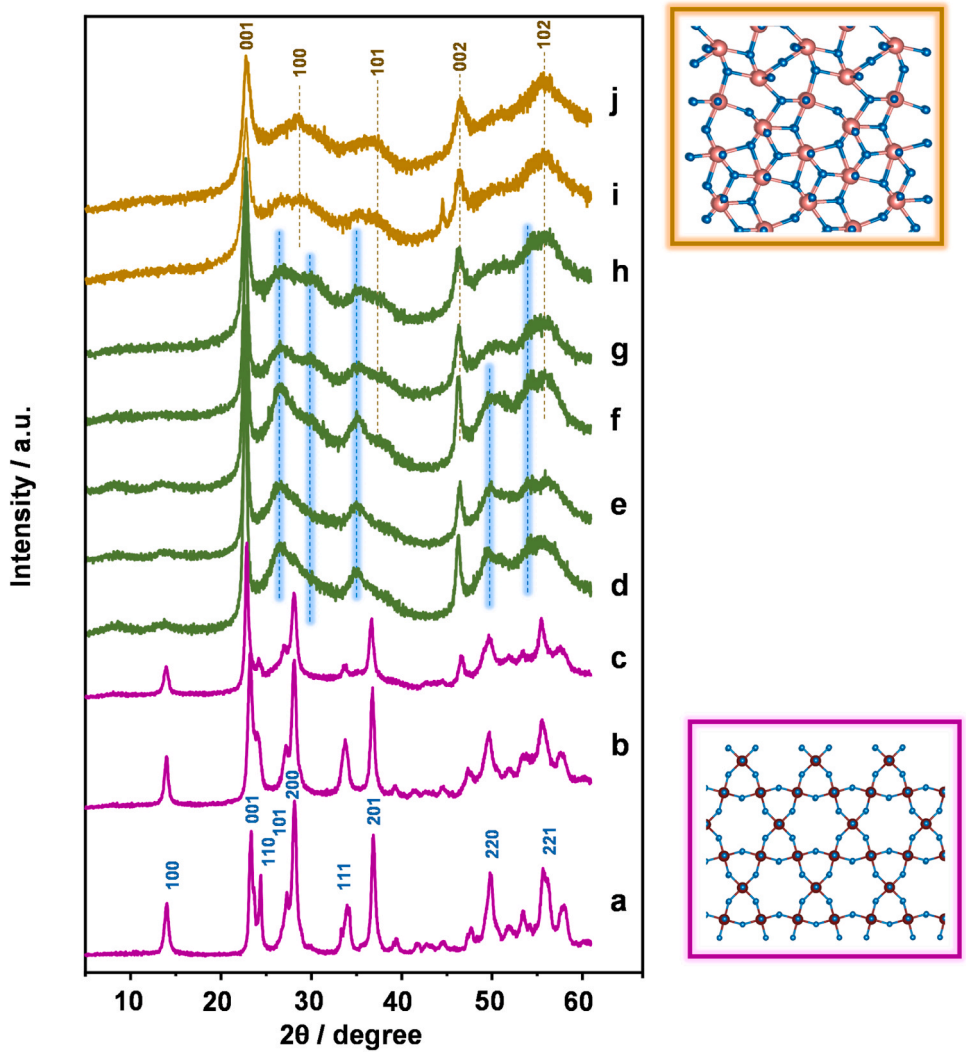

Fig. 1. X-ray diffraction patterns of heat-treated catalysts: a) $\mathbf{W_{1.0}O_x}$; b) $\mathbf{W_{0.90}Nb_{0.10}O_x}$; c) $\mathbf{W_{0.75}Nb_{0.25}O_x}$; d) $\mathbf{W_{0.65}Nb_{0.35}O_x}$; e) $\mathbf{W_{0.50}Nb_{0.50}O_x}$; f) $\mathbf{W_{0.38}Nb_{0.62}O_x}$; g) $\mathbf{W_{0.20}Nb_{0.80}O_x}$; h) $\mathbf{W_{0.10}Nb_{0.90}O_x}$; i) $\mathbf{W_{0.05}Nb_{0.95}O_x}$; and j) $\mathbf{Nb_{1.0}O_x}$. Inserted, the crystal structure of hexagonal tungsten bronze structure (down) and hexagonal niobium oxide (up): oxygen (blue balls); W or Nb (pink balls).

Table 1
Main textural and physicochemical properties of W-Nb-O mixed oxides catalysts.

Catalyst	Composition W/Nb atomic ratio		Acid Sites[c] (μmol_{NH3} g^{-1})	Surface area[d] (m^2 g^{-1})	Surface density of acid sites[e] (μmol_{NH3} m^{-2})
	EDX[a]	XPS[b]			
$W_{1.0}O_x$[f]	1.00/0	1.00/0.00	325.4	16.0	20.3
$W_{0.90}Nb_{0.10}O_x$	0.93/0.07	0.93/0.07	152.7	24.6	6.2
$W_{0.75}Nb_{0.25}O_x$	0.75/0.25	0.74/0.26	159.2	38.2	4.2
$W_{0.65}Nb_{0.35}O_x$	n.d.	n.d.	288.2	67.2	4.3
$W_{0.50}Nb_{0.50}O_x$	n.d.	0.64/0.36	374.9	102.5	3.6
$W_{0.38}Nb_{0.62}O_x$	0.38/0.62	0.43/0.57	331.0	143.9	2.3
$W_{0.20}Nb_{0.80}O_x$	0.20/0.80	0.25/0.75	388.8	134.8	2.9
$W_{0.05}Nb_{0.95}O_x$	0.09/0.91	0.14/0.86	286.1	129.0	2.2
$Nb_{1.0}O_x$	0/1.00	0.00/1.00	171.1	70.0	2.4

[a] Determined by EDS;
[b] Determined by XPS;
[c] Determined by NH_3-TPD;
[d] Determined from N_2 adsorption isotherms (BET method);
[e] Density of acid sites normalized by surface area,
[f] Unlike the rest of the samples heat-treated at 550 °C under N_2, this catalyst was activated at 450 °C under N_2. n.d.= not determined

the results shown in Table 1 confirm that, while the acidity of the sample increases with the Nb content per gram of catalyst, if normalized by surface area, said acidity (also named surface density of acid sites) follows the opposite trend: $W_{0.20}Nb_{0.80}O_x \approx W_{0.38}Nb_{0.62}O_x < W_{0.50}Nb_{0.50}O_x < W_{0.75}Nb_{0.25}O_x < W_{0.90}Nb_{0.10}O_x < W_{1.0}O_X$.

In this sense, to ascertain these Brønsted-Lewis acid differences among samples, NH_3-IR analyses of representative samples were performed, and spectra shown in Fig. 2B confirmed the progressive shift to Lewis acidity when increasing the niobium content of samples. Thus, IR spectrum for $W_{0.90}Nb_{0.10}O_x$ catalyst (Fig. 2B, spectrum a) is mainly composed of a main band centered at ca. 1420 cm^{-1}, related to ammonia cations (NH_4^+) formed by the coordination of NH_3 to Brønsted acid sites [52]. On the contrary, spectra for $W_{0.75}Nb_{0.25}O_x$, $W_{0.38}Nb_{0.62}O_x$ and $W_{0.20}Nb_{0.80}O_x$ samples (Fig. 2B, spectra b, c and d, respectively) show notable bands at 1608 (δ_{as} NH_3), 1265 and 1193 cm^{-1} (due to splitting of the symmetric deformation mode, δ_{sym} NH_3), which have been assigned to Lewis acid sites [52], along with aforementioned 1420 and 1666 cm^{-1}, suggesting also relative amount of Brønsted acid sites, also decreasing in intensity as the niobium content increases (seen particularly in $W_{0.20}Nb_{0.80}O_x$ catalyst). Moreover, NH_3-IR analyses at increased temperatures (from room temperature to 250 °C) are shown in Figure S3, observing in all cases the same band profile although decreasing in intensity, so no changes in the nature of the acid sites can be concluded.

Furthermore, the differences observed in both structural and textural properties of W-Nb-O mixed oxides (see Figs. 1 and 2, and Table 1, respectively) should also correspond to dissimilarities in the morphology of the crystals. Then, Fig. 3 presents the FESEM (Fig. 3A) and HRTEM (Fig. 3B) micrographs of selected W-Nb-O mixed oxides samples.

As can be seen, materials with the highest W content (i.e., $W_{0.90}Nb_{0.10}O_x$ and $W_{0.75}Nb_{0.25}O_x$ samples) display the lowest crystal size, while $W_{0.20}Nb_{0.80}O_x$ and especially $W_{0.05}Nb_{0.95}O_x$ oxides with high Nb contents mainly consist of rather infinitely bigger crystals. In addition to this, shape of HTB-presenting materials (Fig. 3A, micrographs a and b) is clearly cylinder-like, while the loss of the said crystalline structure (observed in Fig. 3A, micrographs c, d and e) leads to more platelet-like shapes [53,54].

On the other hand, HRTEM micrographs observed in Fig. 3B (particularly, micrographs b and c) show for W-Nb-O samples with high Nb content ($W_{0.38}Nb_{0.62}O_x$ and especially $W_{0.20}Nb_{0.80}O_x$) the presence

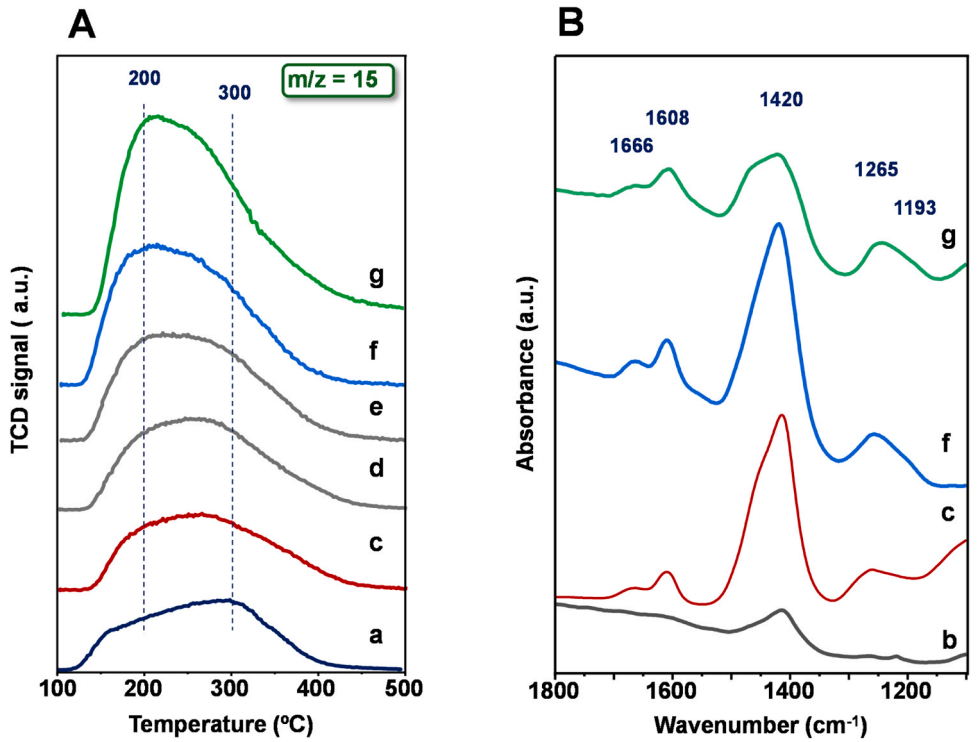

Fig. 2. A) NH_3-TPD profiles of catalysts: a) $W_{1.0}O_x$; c) $W_{0.75}Nb_{0.25}O_x$; d) $W_{0.65}Nb_{0.35}O_x$; e) $W_{0.50}Nb_{0.50}O_x$; f) $W_{0.38}Nb_{0.62}O_x$; and g) $W_{0.20}Nb_{0.80}O_x$. **B)** NH_3-IR spectra at room temperature of: b) $W_{0.90}Nb_{0.10}O_x$, c) $W_{0.75}Nb_{0.25}O_x$, f) $W_{0.38}Nb_{0.62}O_x$ and g) $W_{0.20}Nb_{0.80}O_x$ catalysts.

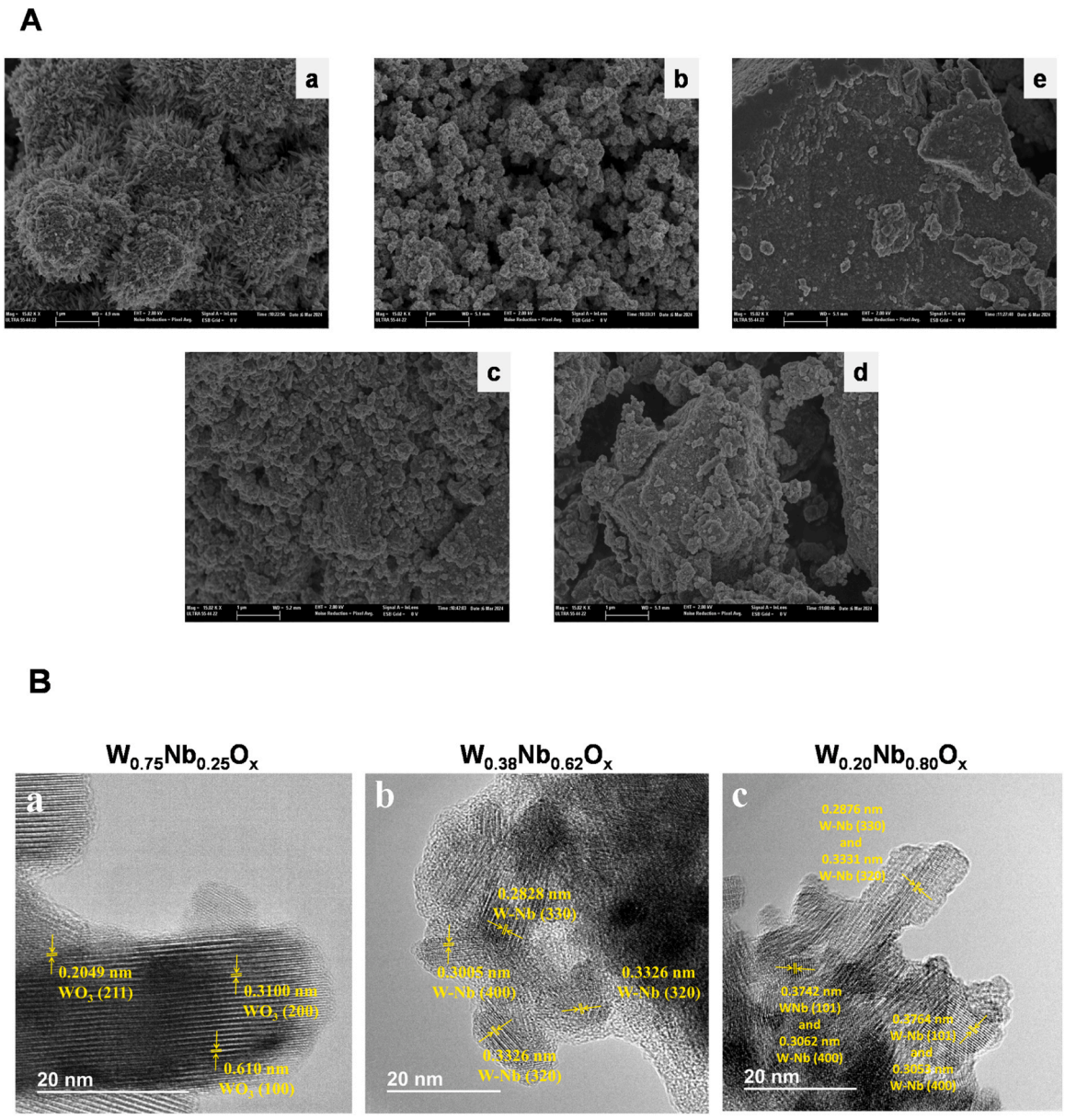

Fig. 3. A) FESEM micrographs at 15k magnification of: a) $\mathbf{W_{0.90}Nb_{0.10}O_x}$; b) $\mathbf{W_{0.75}Nb_{0.25}O_x}$; c) $\mathbf{W_{0.38}Nb_{0.62}O_x}$; d) $\mathbf{W_{0.20}Nb_{0.80}O_x}$; and e) $\mathbf{W_{0.05}Nb_{0.95}O_x}$. **B)** HRTEM micrographs of selected samples: a) $\mathbf{W_{0.75}Nb_{0.25}O_x}$, b) $\mathbf{W_{0.38}Nb_{0.62}O_x}$ and c) $\mathbf{W_{0.20}Nb_{0.80}O_x}$.

of metal oxides phases with interplanar distances in between WO_3 and Nb_2O_5 oxides that could be assigned to different planes (i.e., (330), (320), (400), and others) of W-Nb-O mixed oxides. On the contrary, the presence of W oxide phases with only interplanar distances assigned to planes (200), (211) and (100) of WO_3 are observed for the measured sample with low Nb content ($\mathbf{W_{0.75}Nb_{0.25}O_x}$, see Fig. 3B, picture a). All these evidences confirm the presence of W-Nb-O mixed oxides structures when Nb content in the solids increased upper a W/Nb molar ratio of 0.30.

Further spectroscopic characterization results are displayed in Fig. 4, where confocal Raman studies of some representative catalysts are presented. Moreover, FTIR analyses of selected samples, both as-synthesized and heat-treated, and the attained spectra are plotted in Figure S4. The IR spectra of activated catalysts (Fig. S4-B), in the 1850–400 cm^{-1} region, present main bands in the 1000–400 cm^{-1} region, which correspond to both Me=O (in the 1000–900 cm^{-1} region) and Me-O-Me stretching modes (in the 900–400 cm^{-1} region) in this type of bronze-like materials [55,56]. In addition, a small band at ca. 1400 cm^{-1} is only observed for sample $\mathbf{W_{1.0}Ox}$, heat-treated at 400 °C, and related to the $\delta_{(NH)}$ deformation modes of NH_4^+ cations [56]. This suggests that, in this case, ammonium cations are not completely removed during the material activation at 400 °C. Moreover, the presence of different bands in the 1500–1800 cm^{-1} region in as-synthesized samples with the highest niobium content (Fig. S4-A) has been associated with oxalate species that, in any case, disappear after the thermal activation [57].

Confocal Raman analyses were performed in the samples to provide accurate compositional information at a local microscale level [58]. In this context, optical micrographs, Raman intensity images in the XY plane, and the average Raman spectra are presented in Fig. 4, derived from representative areas for each sample. Raman mappings reveal a single-phase composition, as only one spectrum is detected throughout each sample, obtained from the scanned area indicated by an orange box (Fig. 4). Furthermore, $\mathbf{Nb_{1.0}O_x}$ and $\mathbf{W_{1.0}O_x}$ samples has been also included as references. Accordingly, six distinct Raman bands can be clearly observed in the Nb-doped WO_3 samples, all associated with the

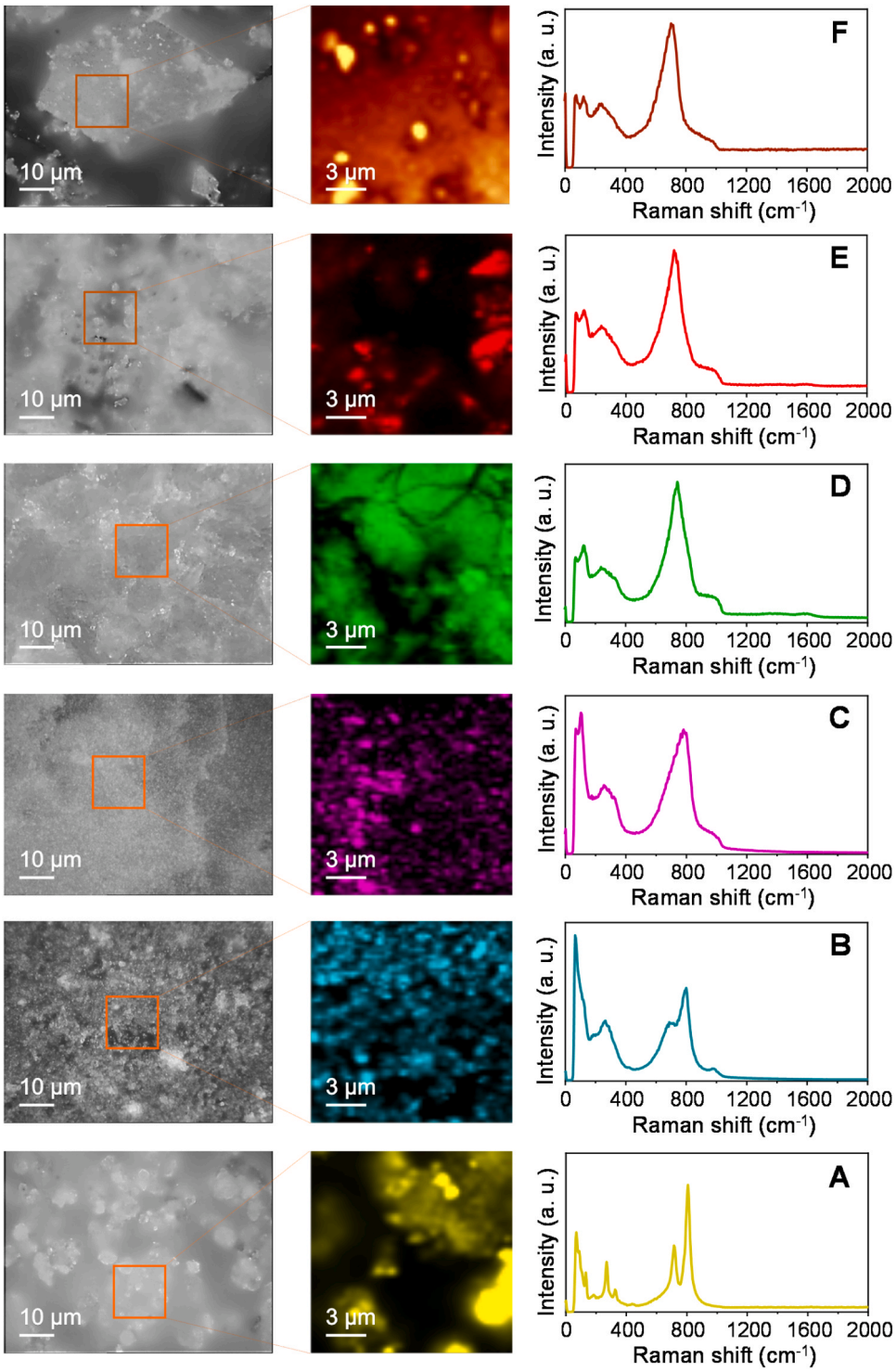

Fig. 4. Optical micrographs (left), in-plane Raman intensity images (center) and Raman spectra right) of a) $\mathbf{W_{1.0}O_x}$; b) $\mathbf{W_{0.90}Nb_{0.10}O_x}$; c) $\mathbf{W_{0.75}Nb_{0.25}O_x}$; d) $\mathbf{W_{0.38}Nb_{0.62}O_x}$; e) $\mathbf{W_{0.20}Nb_{0.80}O_x}$; and f) $\mathbf{Nb_{1.0}O_x}$. The yellow square area of the optical micrographs indicates the region of the acquired Raman mapping.

presence of a hexagonal WO_3 structure [59]. This is noteworthy because XRD results for the $\mathbf{W_{0.38}Nb_{0.62}O_x}$ and $\mathbf{W_{0.20}Nb_{0.80}O_x}$ samples did not show the formation of the said HTB structure (Fig. 1A). Nevertheless, some differences can be ascertained among samples.

In the $\mathbf{W_{0.90}Nb_{0.10}O_x}$ sample, the signal at approximately 124 cm^{-1} can be attributed to MeO_6 (where Me = W, Nb) lattice vibrations as a whole, shifting to higher frequencies with increasing Nb content in the catalyst. This suggests a progressive contraction in the lattice parameters of samples with higher Nb content [60]. Furthermore, Raman bands at approximately 235 and 324 cm^{-1} are associated with deformations of Me-O bonds, while bands at around 720 and 799 cm^{-1} are assigned to O-Nb-O and O-W-O vibrations, respectively, with the former increasing with the Nb content. Finally, a broad band at approximately 994 cm^{-1} is ascribed to O=Me stretching vibrations and no noticeable variations are detected. These Raman mode positions are consistent with other studies on Nb- and W-based oxide samples [61–64].

Surface composition of the catalysts was studied by means of XPS,

and results are shown in Table 1 and Figure S5. Considering tungsten species, all samples at *4 f* core level display a doublet at ca. 35.5 eV (*4 $f_{7/2}$*) and 37.6 eV (*4 $f_{5/2}$*) related to the presence of W^{6+} species [62]; while niobium *3d* core level can be deconvoluted into a single doublet at ca. 207.1 eV (*$3d_{5/2}$*) and 209.8 eV (*$3d_{5/2}$*), assigned uniquely to Nb^{5+} species [65].

Nevertheless, minority presence of W^{5+} species among these samples is always observed. However, in the case of the sample with the lowest tungsten content (i.e., $\mathbf{W_{0.05}Nb_{0.95}O_x}$ catalyst), a significant amount of partially reduced W^{5+} species (ca. 40 %) can be deconvoluted, provided that in this case the lattice must be mainly formed of Nb^{5+} species. Interestingly, EDS and XPS compositions were shown to be highly similar, suggesting a strong homogeneity of the different catalysts, especially those with high W-contents. Nonetheless, for Nb-rich catalysts, an increase in the tungsten content on the surface of the samples compared to the bulk composition has been observed (see Table 1).

3.2. Catalytic activity results

3.2.1. Preliminary catalytic tests

As previously mentioned, the dehydration reaction of xylose to furfural is industrially carried out using sulfuric acid as a homogeneous catalyst, typically achieving furfural selectivities of around 70 %. For example, in the case of Huaxia/Westpro plants currently operating in China, 25–35 tons of steam are consumed per ton of furfural produced, by reaching ≈ 50 % furfural yields based on the theoretical pentosan content [20]. Nevertheless, in order to figure out the catalytic behavior of H_2SO_4 under our operational conditions (see above in Experimental procedure, Section 2.4.), some preliminary tests were carried out using different aqueous solutions of sulfuric acid as homogeneous catalyst for the dehydration of xylose to furfural in autoclave-type reactors. Therefore, Fig. 5 shows the evolution of xylose conversion and the selectivity to furfural with time using two different acid concentrations, 1 and 5 wt % (Figs. 5A and 5B, respectively) at 160 ºC, while additional experiments at different reaction temperatures are plotted in Figure S6, showing that best results are achieved at 160 ºC.

In this sense, a clear effect on the catalytic activity is observed as a function of sulfuric acid concentration. Then, a xylose conversion of roughly 65 % is obtained by using 1 wt% of H_2SO_4 (Fig. 5A) after one hour, with a maximum of 80 % after three hours of reaction. However, xylose conversion can be also increased when increasing the sulfuric acid concentration (Fig. 5B) by achieving ca. 85 % after one hour, and reaching full conversion after two hours of reaction. Nevertheless, and regarding the furfural selectivity, no big differences can be ascertained during the first hour of reaction in both cases. Thus, it is observed a sudden increase up to 80–90 % selectivity for reaction times lower than 30 min, followed by a decrease up to ca. 40 % within the first hour. Interestingly, when a lower H_2SO_4 concentration (Fig. 5A) was used, this furfural selectivity is maintained throughout the reaction, whereas the selectivity to furfural further drops to ca. 20 % by increasing the H_2SO_4 concentration up to 5 wt% (Fig. 5B), this suggesting a larger production of by-products in the latter case mainly related to consecutive reactions between furfural and intermediates. In any case, about 45 % yield to furfural is obtained using H_2SO_4 as catalyst in the best case, a similar result obtained in other investigations [66].

Furthermore, it is worth noting that the acid catalyzed xylose dehydration goes through intermediates formation giving furfural as main product if the catalyst offers the adequate acidity, but intermediates can also rapidly undergo non-desired reactions (i.e., condensation, resinification) if active sites have stronger or weaker acidity than required (see Scheme 1). In general, the main by-product observed under the reaction conditions here tested are humins (polymeric compounds with solid and dark appearance), together with very small amounts of other side-products produced by further degradation via hydrolysis/dehydration of xylose, such as formic and acetic acid, formaldehyde and acetone, among others.

On a further step, and with the aim of using solid heterogeneous acid catalysts for the xylose dehydration reaction, different commercially available heterogeneous catalysts such as Amberlyst-15® polymeric resin, H-Beta and H-USY zeolites, as well as WO_3 and Nb_2O_5 commercial oxides were tested, and comparative results can be found in Table 2. In that table, water and H_2SO_4 were used as reference homogeneous catalysts for comparative purpose. Results showed that, even though acceptable furfural productions were obtained for Amberlyst-15® and H-USY catalysts, selectivity values are still far from H_2SO_4 performance. Nevertheless, the Amberlyst-15® catalyst presents several regeneration problems [67], while in the case of H-USY catalyst difficulties in the separation of the solid catalyst from the reaction mixture (slurry solution containing huge amount of oligomers/humins) are encountered (see Figure S8 in SI), these important drawbacks making them unsuitable for this process. Additionally, H-Beta zeolite along with Nb_2O_5 and WO_3 oxides reported remarkably low furfural selectivity values (more than three times lower compared to sulfuric acid at one hour of reaction time). On the other hand, even commercial WO_3 and Nb_2O_5 simple oxides presented low activity and selectivity to furfural, it has been previously reported that mixed W-Nb-O oxides with either hexagonal or pseudo-crystalline bronze type structure and presenting tunable Brønsted/Lewis acid sites ratio depending on the chemical composition are of special interest in different biomass transformation reactions [42–44]. Therefore, a detailed study of these mixed oxides is presented here next.

3.2.2. Dehydration of xylose to furfural over W-Nb-O mixed oxides

It is well known that a suitable combination of Brønsted/Lewis acid

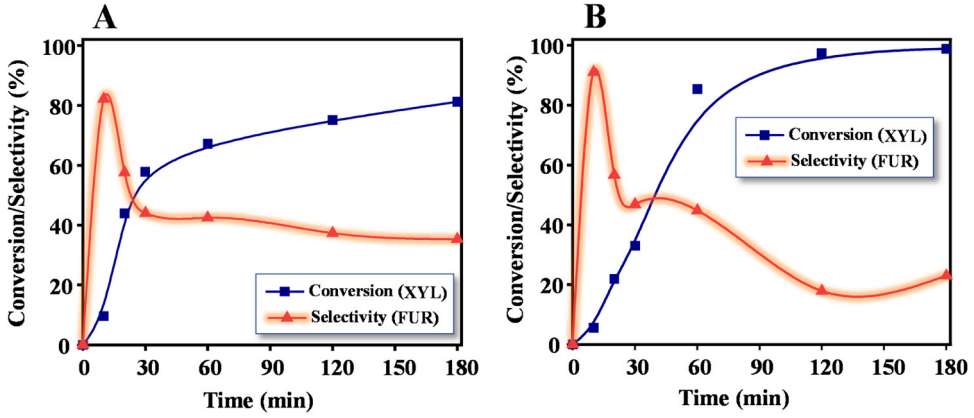

Fig. 5. Xylose dehydration to furfural using H_2SO_4 aqueous solution as homogeneous catalyst: **A)** 1 wt% of H_2SO_4; **B)** 5 wt% of H_2SO_4. Reaction conditions: 10 wt% Xylose, 4 mL H_2O, at 160 °C with 1000 r.p.m.

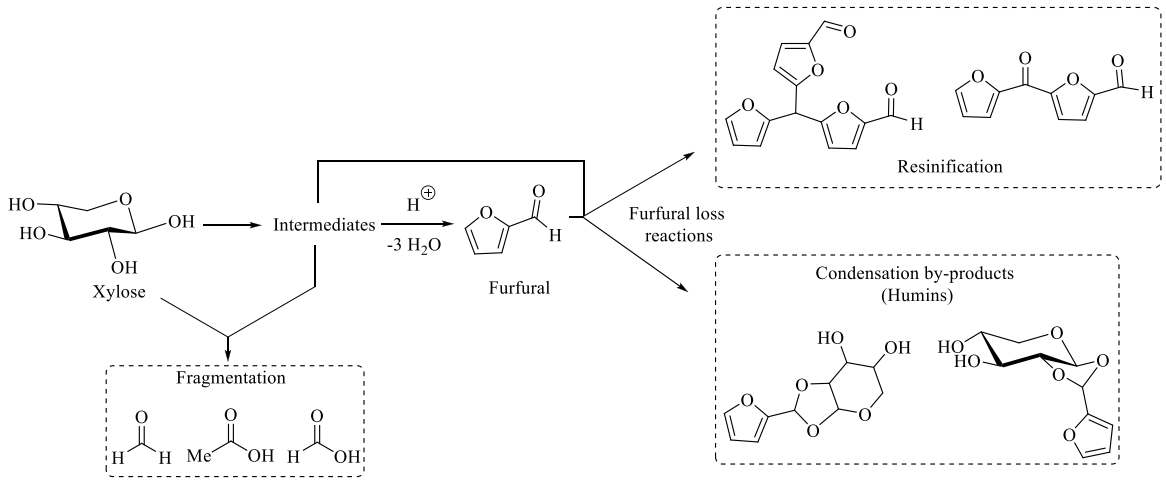

Scheme 1. Furfural synthesis via dehydration of xylose and plausible main by-products.

Table 2
Xylose dehydration to furfural using different commercially available heterogeneous catalysts compared to H_2SO_4.[a].

Catalyst	t = 10 min		t = 60 min	
	Xylose Conversion (%)	Furfural Selectivity (%)	Xylose Conversion (%)	Furfural Selectivity (%)
HWT[b]	n.d.	n.d.	4.1	87.3
H_2SO_4	5.6	91.1	85.4	44.8
Amberlyst−15®	41.8	12.5	99.7	33.7
H-Beta	8.9	11.1	29.0	8.0
H-USY	n.d.	n.d.	99.1	33.3
WO_3	49.5	12.1	69.5	13.6
Nb_2O_5	46.5	10.9	80.8	14.5
$W_{0.38}Nb_{0.62}$	44.4	18.0	91.2	32.3

[a] Reaction conditions: 10 wt% Xylose, 4 mL H_2O, at 160 °C with 1000 r.p.m., for 10 or 60 min. Amount of catalyst: 0.04 g for homogeneous catalyst (H_2SO_4) and 0.16 g for solid catalyst.

[b] HWT: Hot water treatment, reaction without catalyst at 160 ºC. n.d.= not determined.

sites with the adequate strength can enhance the dehydration reaction of xylose to furfural [68]. Thus, and considering the catalytic results previously attained with WNb-based acid catalyst (see Table 2), different W-Nb-O mixed oxides with different physicochemical characteristic (Table 1) were tested to study the influence of the chemical composition on the selective dehydration of xylose to furfural and results are shown in Fig. 6 and Table 3. It is important to mention that the main reaction parameters (temperature, amount of catalyst, and solvent) of the process have been previously optimized, and results from this optimization are shown in Table S1 (in Supporting Information).

Catalytic results for the dehydration of xylose to furfural over the synthesized W-Nb-O catalysts show two different trends (Fig. 6A). On the one hand, for the catalysts with none to low niobium content (i.e., ***h*-WO_3**, $\mathbf{W_{0.90}Nb_{0.10}O_x}$ and $\mathbf{W_{0.75}Nb_{0.25}O_x}$ samples which present the HTB structure, see Fig. 1), xylose conversion values tend to increase with the niobium content while uncorrelated furfural selectivity were encountered. Nevertheless, by further increasing the niobium content and therefore losing the HTB crystalline structure (from $\mathbf{W_{0.65}Nb_{0.35}O_x}$ sample) an increase in both xylose conversion and furfural selectivity is observed, reaching a maximum for the $\mathbf{W_{0.20}Nb_{0.80}O_x}$ catalyst, with 96.1 % xylose conversion and 38.8 % selectivity to furfural. Interestingly, these values resulted in a 37.3 % furfural yield, comparable to homogeneous H_2SO_4 catalyst (i.e., 38.3 %) under similar reaction conditions (see Table 3 and Fig. 6).

Then, apart from the differences in the crystalline structure among samples, the different incorporation of niobium into the framework also leads to a tunable Brønsted/Lewis ratio, as observed in Figs. 2A and 2B, with an evident increase in the amount of Lewis acid sites (see Fig. 2B) concomitantly with the niobium content.

Likewise, the different furfural yields can also be related to the relative amount of acid sites on the surface of the catalyst and their adequate distribution on the solid. In this manner, it was also reported that the loss of the HTB structure in these WNb-based oxides provokes an increase in the specific surface area (see Table 1). In this sense, the furfural yield and both the surface area and the surface density of acid sites are represented in Figs. 6B and 6C, respectively, as a function of the chemical composition of the W-Nb-O samples. It was found that the surface density of acid sites decreased as the niobium content increased, reaching a plateau from $\mathbf{W_{0.38}Nb_{0.62}O_x}$ to $\mathbf{W_{0.05}Nb_{0.95}O_x}$ samples, while the furfural yield followed the opposite trend, achieving a maximum value (ca. 38 %) for $\mathbf{W_{0.20}Nb_{0.80}O_x}$ sample, that corresponds also to the higher total acidity and surface area (see Fig. 6B) for the catalysts studied. These two different trends suggests that not only a proper amount of Brønsted/Lewis acid sites is needed for the effective xylose dehydration to furfural to occur, but also these acid sites should be somehow dispersed in a suitable environment to avoid consecutive or secondary reactions between furfural and intermediates conducting to the formation of by-products, such as humins in our reaction conditions.

In order to provide more insights on the adequate Brönsted/Lewis acid sites ratio and its influence of the catalyst behavior, calculations from acidity measurements of four selected W-Nb-O materials performed by NH_3-TPD (see Fig. 2A) and NH_3-IR (see Figure S3) were done. With the deconvolution of bands of NH_3-TPD spectra of W-Nb-O samples two main peaks centered approximately at 200–210 ºC (A1) and 300–330 ºC (A2), commonly assigned to Lewis (A1) and Brönsted (A2) acid sites, respectively, were determined (see Figure S9 in SI). The integration of these peaks revealed that Lewis/Brönsted ratio increases with the Nb incorporation on the Bronze structure of W-Nb-O mixed oxides, going from 1.55 for $W_{0.75}Nb_{0.25}$ sample to 2.16 for the $W_{0.20}Nb_{0.80}$ optimum catalyst. This increasing in Lewis/Brönsted acid sites also correlates with the catalytic performance for these samples, thus evidencing the presence of more Lewis acid sites in the catalyst is relevant for the xylose dehydration process. This affirmation is reinforced by the amount of Lewis and Brönsted acid sites present in the mixed oxides calculated from data of NH_3-IR spectra of the same four selected W-Nb-O samples (see Fig. 2B and Table S3 in SI). The attained results confirmed that the presence of Lewis acid sites increases with the Nb content in the materials, this correlating with the increase in the catalytic activity observed with a maximum in furfural yield for the $W_{0.20}Nb_{0.80}$ optimum catalyst.

At this point, the specific role of Brönsted and Lewis acid sites on the

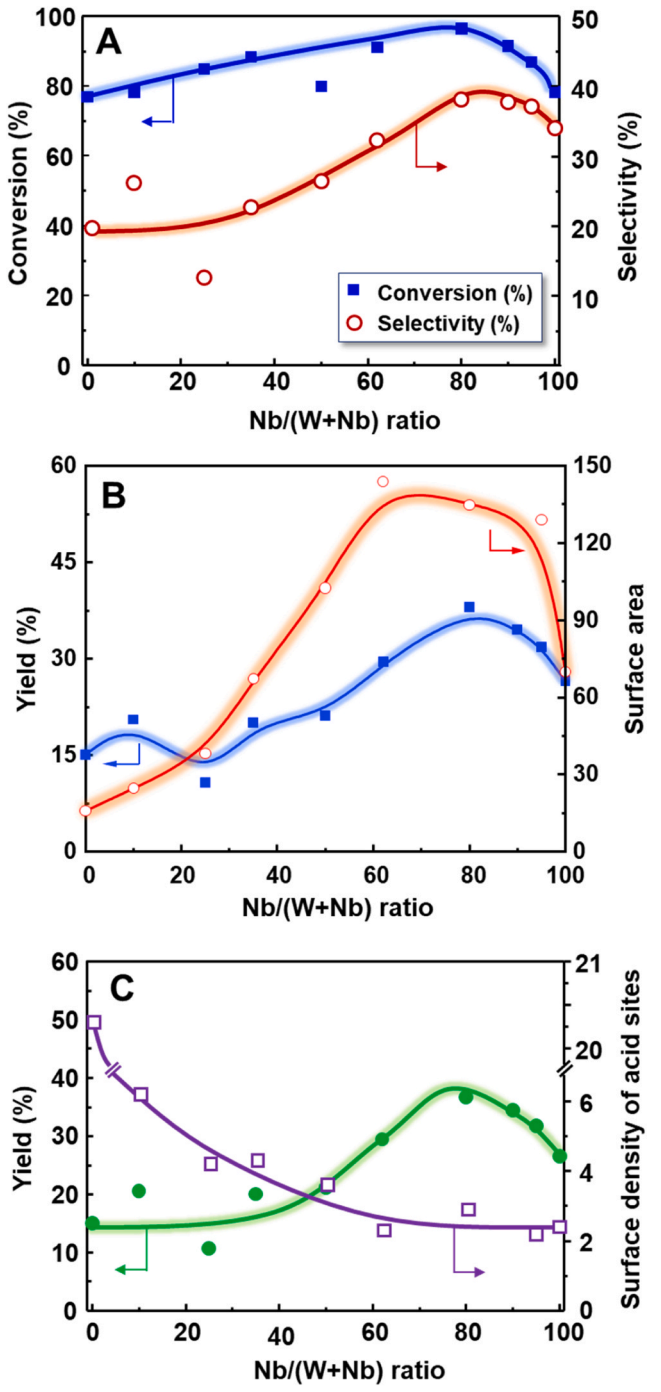

Fig. 6. Xylose conversion and selectivity to furfural at 1 h of reaction (A); furfural yield and surface area (B); and furfural yield and surface density of acid sites (C) as a function of the chemical composition of materials (i.e., Nb/(W/+Nb) ratio). Reaction conditions: 10 wt% Xylose, 160 mg catalyst, 4 mL H_2O, at 160 °C with 1000 r.p.m.

reaction mechanism of xylose-to-furfural dehydration is difficult to assess, this fact being still a matter of debate among the researchers. In general, there are two main reaction mechanisms proposed in literature, which involve the direct route and the indirect route, respectively, for furfural production from xylose (see Figure S10 and its explanation in SI). In the direct route, also called cyclic pathway, first protonation step followed by H_2O elimination and 5-member cycle rearrangement (that could be concerted steps) with a further furan ring formation to give furfural is the most widely accepted synthetic way. In the indirect route

Table 3
Xylose dehydration to furfural over selected W-Nb-O catalysts with different W/Nb ratio.[a]

Catalyst	t = 10 min		t = 60 min	
	Xylose Conversion (%)	Furfural Selectivity (%)	Xylose Conversion (%)	Furfural Selectivity (%)
H_2SO_4	5.6	91.1	85.4	44.8
$W_{1.0}O_x$	55.7	24.5	76.9	19.7
$W_{0.90}Nb_{0.10}O_x$	57.1	21.5	78.3	26.7
$W_{0.38}Nb_{0.62}O_x$	44.4	18.0	91.2	32.3
$W_{0.20}Nb_{0.80}O_x$	47.5	49.3	96.1	38.8
$Nb_{1.0}O_x$	41.0	25.8	78.2	34.3

[a] Reaction conditions: 10 wt% Xylose, 4 mL H_2O, at 160 °C with 1000 r.p.m., for 10 or 60 min. Amount of catalyst: 0.04 g for homogeneous catalyst (H_2SO_4) and 0.16 g for solid catalyst. H_2SO_4 data for comparison.

(thermodynamically disadvantaged), the first step conduct to a xylose transformation to its open chain form that then isomerize to xylulose, which after a rearrangement to 5-member ring is protonated and finally dehydrated (H_2O elimination) to produce furfural (see Figure S10 and its explanation in SI). In this sense, it is widely accepted in literature that Brönsted acids are the main responsible of first steps of reaction (protonation and H_2O elimination) when reaction occurs through the proposed direct route, the assistant role of Lewis acid sites in the ulterior steps of rearrangement and furanic ring formation is more plausible. This later Lewis acid assistance could explain the better selectivity observed to the furfural formation when comparing with other solid acid catalysts. On the other hand, the indirect route could also be directed by Brönsted acid sites (mainly in the first step of xylose opening to chain form) with assistance of Lewis acid sites in the isomerization to xylulose and further cyclization, although the two final steps (protonation and H_2O elimination) is most likely catalyzed by Brönsted acids [69].

Attending to all the above-mentioned and here attained results, we believe that in our case the reaction takes place preferably by the cyclic transformation of xylose to furfural (direct route), this route being favored by the presence of Brönsted acid sites with the assistance of Lewis centers. On the other hand, the occurrence of the indirect route type mechanism via isomerization of xylose to xylulose and further formation of furfural could not be ruled out. In fact, the formation of a small amount of xylulose as reaction intermediate has been observed in chromatographic analyses during our catalytic experiments (see Figure S11 in SI). These results are similar to those found in literature, for example in the research of Sixta et al. [69], where they observed the appearance of traces of xylulose when carrying out the dehydration reaction of xylose to furfural. These experimental evidences indicate that both mechanisms could coexist; although presumably the reaction mainly occurs by direct dehydration (cyclic pathway), as xylulose formation takes place in lesser extent.

3.2.3. Study on the stability and reusability of W-Nb-O catalyst under reaction conditions

Furthermore, the stability and reusability of this type of oxides was studied by using the best performing catalyst, this is the $\mathbf{W_{0.20}Nb_{0.80}O_x}$ sample (see Fig. 7 and Table S2, in Supporting Information). In this case, the dehydration of xylose to furfural was evaluated using a mixture of H_2O/ethanol as mono-phasic solvent system. In fact, the effect of using different solvents either in mono-phasic (H_2O/ethanol) or bi-phasic (H_2O/toluene) systems was previously assessed for a representative W-Nb-O catalyst (see Table S1 in SI). Results indicated that while the employment of H_2O/toluene bi-phasic solvent system drastically decreased the catalytic activity, the use of H_2O/ethanol mono-phasic solvent system showed a little enhancement in the selectivity (and consequently in yield) to furfural, probably due to the formation of xyloside-type ethers intermediates [70] (see Table S1). Therefore, catalytic recycling tests over the sample that showed the best catalytic

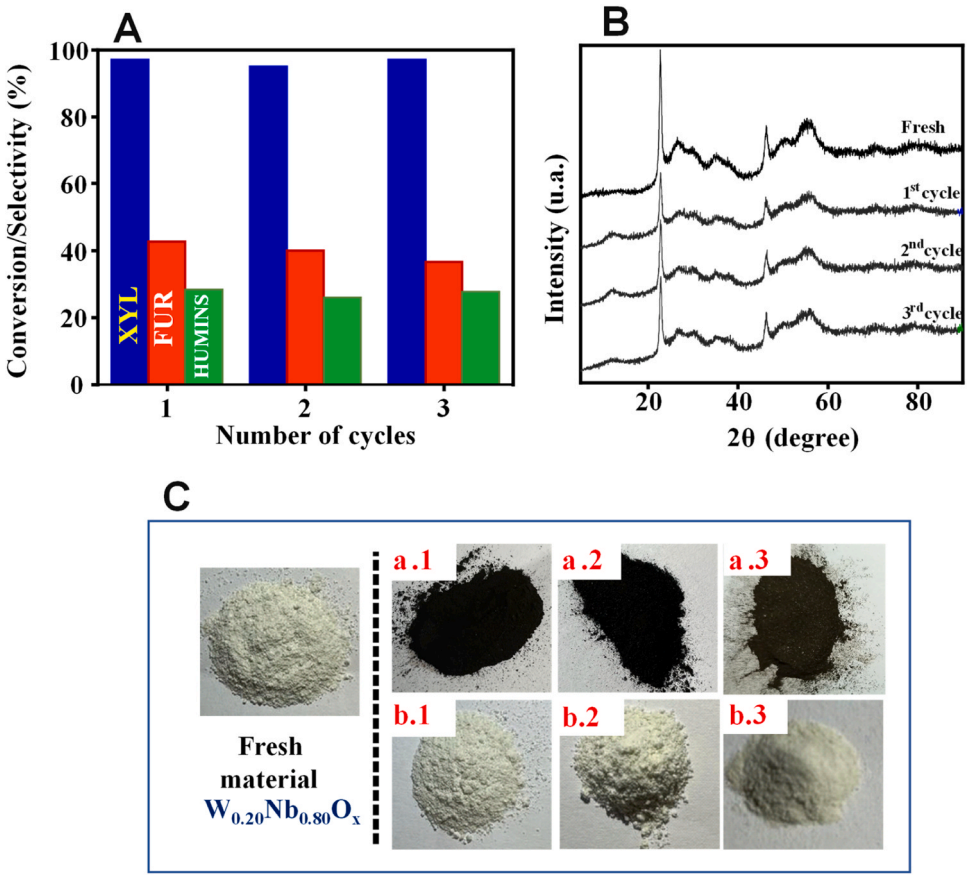

Fig. 7. A) Xylose conversion (blue) and selectivity to furfural (red) and humins (green) on $W_{0.20}Nb_{0.80}O_x$ catalyst; **B)** XRD patterns of fresh and regenerated catalysts after catalytic cycles; and, **C)** fresh and regenerated catalyst in nitrogen (**a.x.**) or air (**b.x.**) stream after the first, second and third catalytic cycle for $W_{0.20}Nb_{0.80}O_x$ sample.

performance, this is $W_{0.20}Nb_{0.80}O_x$ material, were carried out by using the H_2O/EtOH solvent system at 160 °C (with 10 wt% xylose and 160 mg of catalyst). After each catalytic cycle, the solid catalyst was recovered from reaction mixture, washed with a H_2O/EtOH mixture, and then regenerated in air at 550 °C for two hours before its use in the next catalytic cycle.

Accordingly, the results in terms of xylose conversion and main products selectivity obtained for three catalytic cycles using the $W_{0.20}Nb_{0.80}O_x$ oxide are shown in Fig. 7A. There, it can be seen that the catalyst maintained practically the same catalytic activity, with xylose conversion ranging always between 95 % and 98 %, while the furfural selectivity suffered a little decrease with consecutive catalytic reuses, although not very noticeable, while humins products did not change so much after any reuse. Detailed results are displayed in Table S2.

Characterization measurements performed on the fresh and used catalysts after recycling tests shown in Fig. 7B and Table S2 demonstrated that both the structural and chemical stability was maintained after every "use + regeneration" cycle, as no changes were ascertained either by XRD patterns (Fig. 7B) or by metal contents data from ICP (in Table S2) measured before and after each catalytic cycle. In addition, the humins deposits formed onto the solid catalyst during reaction have been quantified, and for this purpose, all the solids present in the reaction crude (catalyst + humins) have been recovered and washed with H_2O/EtOH and later analyzed by both EA and TGA. Table S2 also shows the differences in the Carbon content of the catalyst before and after regeneration, where a complete elimination of the accumulated humins on the catalyst surface can be appreciated.

It is interesting to mention that the regeneration step was also carried out under N_2 stream, however, the presence of O_2 is mandatory to eliminate the humins deposists as it can be seen in Fig. 7C, where only the catalyst regenerated under air stream recover its original physical appearance. Nevertheless, a complete humins removal is unlikely to exist, suggesting that this is reason for the very slight decrease in furfural selectivity after every catalytic cycle. In any case, the $W_{0.20}Nb_{0.80}O_x$ material proves to be a robust and efficient catalyst for the selective dehydration of xylose to furfural by working at relatively high xylose concentrations in aqueous mono-phasic solvent systems under moderate reaction conditions.

Finally, the stability over time of these W-Nb-O mixed oxides was studied by submitting a representative sample ($W_{0.38}Nb_{0.62}O_x$) to the optimal reaction conditions during 14 days, in order to identify possible changes in the structure of the catalyst. As shown in Fig. 8, the structure of the catalyst determined by X-ray diffraction measurements is very similar to the fresh material; moreover, the chemical composition (W/Nb ratio) measured by ICP shows very small changes in the W/Nb ratio, and the absence of Nb and W in the liquids after reaction. Therefore, the catalyst demonstrated to be a highly resistant and robust material under hydrothermal conditions and under common operational conditions employed for synthesis of furfural through dehydration of C5 sugars.

3.2.4. Comparative analysis of results obtained over W-Nb-O mixed oxides and other reported solid acid catalysts

With the aim to evaluate the catalytic performance of our developed W-Nb-O mixed oxides in the C5 sugar (xylose) dehydration to furfural within the actual context, a comparison of our catalytic results (in terms of reaction conditions, reusability and furfural productivity) with those observed for other catalytic systems, (i.e., some of the most relevant solid acid catalyst recently reported in literature) is presented in Table 4.

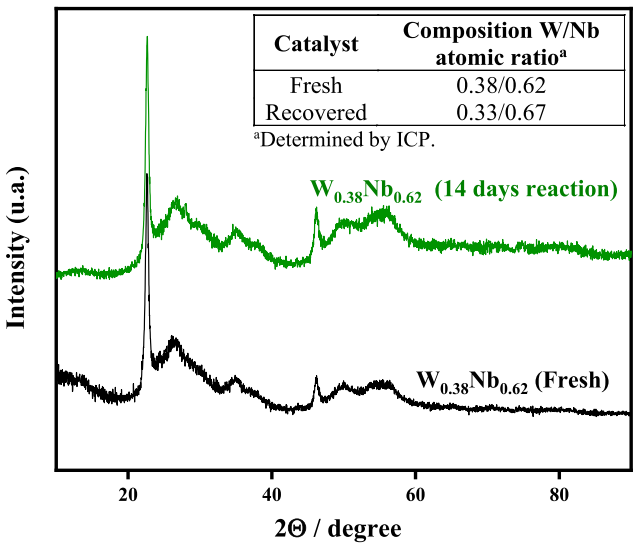

Fig. 8. XRD patterns of $W_{0.38}Nb_{0.62}O_x$ regenerated material obtained before and after 14 days reaction (stability test) of xylose dehydration to furfural. Inset: Catalyst composition (W/Nb ratio) before and after the stability test. Reaction conditions: 10 wt% Xylose, 4 mL solvent (1 mL_{H2O} / 3 mL_{EtOH}), 160 mg $W_{0.38}Nb_{0.62}O_x$, at 160 °C with 1000 r.p.m. Regeneration conditions: at 550 ºC, 1 h in air + 2 h in N_2.

In this case, we are also including comparative results attained with sulfuric acid (homogeneous reaction). As expected, results indicated that furfural productivities (calculated as $g_{Fur}•g_{Cat}^{-1}•h^{-1}$) are higher for the homogeneous system than for the solid catalysts, due to the fact that calculations/estimations were made considering the mass of mineral acid and not the amount or concentration of Brönsted acid sites. It also worth noting that, except with the here reported catalytic system, carbon balances in reactions were neither considered not reported in all the cases, this pointing out the lack of accuracy of some of the results compiled for other solid catalysts in Table 4.

On one hand, medium pore H-ZSM-5 [35] zeolites working in biphasic (water/toluene) system gave *a priori* 82.4 % furfural yield, with a moderate furfural productivity (0.436 $g_{Fur}•g_{Cat}^{-1}•h^{-1}$), but the way or method for determining the latest results are not well described or specified by the authors.

On the other hand, Nb-containing catalysts have been also proposed [31,36–38]. Niobium oxide supported on MCM-41 (denoted as MCM-Nb16) [36] catalyst used with a biphasic water/toluene solvent system yielded around 60 % of furfural, with a productivity value of 0.383 $g_{Fur}•g_{Cat}^{-1}•h^{-1}$). However, in the latter case, as well as for eHTiNbO$_5$-MgO [31] and for a microporous niobium silicate denoted as H-AM11 [37] solid acid catalysts, the sugar concentration employed was relatively low (<3.2 wt%), as low were also the furfural productivities achieved even working in biphasic (water/toluene) solvent system (see Table 4).

In addition, 68 % furfural yield could be reached with Nb_2O_5-type catalyst using water/CPME monophasic solvent system [38], although the calculated furfural productivity was 0.218 $g_{Fur}•g_{Cat}^{-1}•h^{-1}$ in this case. We must indicate that lower furfural productivities (<0.215 $g_{Fur}•g_{Cat}^{-1}•h^{-1}$) were attained by using other Nb-based catalysts under monophasic solvent systems [71,72]. However, in general, lower furfural productivities were achieved with solid acid catalysts working in monophasic solvent systems when comparing with results obtained with solid acid catalyst in water/toluene biphasic system [30,35,36].

Remarkably, the here developed W-Nb-O mixed oxides catalyst, prepared hydrothermally and heat-treated at 550ºC, working in monophasic water/EtOH solvent system offered the best value of furfural productivity (0.683 $g_{Fur}•g_{Cat}^{-1}•h^{-1}$) from all the solid acid catalysts listed in Table 4, better than that of Nb_2O_5 catalyst in biphasic H_2O/Toluene system (productivity = 0.640 $g_{Fur}•g_{Cat}^{-1}•h^{-1}$) [30], and much better than the other solid acids analyzed (productivity ranging between 0.073 and 0.436). Furthermore, although the furfural yield was moderate (41.4 %), this value was attained at just 1 h of reaction, by employing 9.1 % concentration of sugar at low temperature (160 ºC), while calculated carbon balances for the reaction were > 75 %, values not informed by any other report in literature. More importantly, the robustness and reusability of the catalyst was also demonstrated, with only 5 % yield loss after 3 consecutive catalytic cycles.

Summarizing, the here reported W-Nb-O mixed metal oxides showed

Table 4
Composition of catalytic results, reaction conditions, reusability and calculated furfural productivities of most recent reported solid catalysts vs the W-Nb-O catalyst here studied in the sugar (xylose) dehydration to furfural.

Characteristics of reaction	Catalyst	Solvent system	Time (min)	Sugar conc. (wt%)	Productivity ($g_{Fur}•g_{Cat}^{-1}•h^{-1}$)	Reusability		Temp (ºC)	Yield (%)	CB (%)	Ref.
						N° of cycles	Yield loss (%)				
Industrial catalyst	H_2SO_4	H_2O	60	9.1	4.898	-	-	160	38.3	41	***This work***
	H_2SO_4	H_2O	180	10.0	4.913	-	-	170	46.1	N.d.	1
	H_2SO_4	H_2O/ Toluene	300	10.0	1.060	-	-	120	83.0	N.d.	2
Biphasic Catalyst	ZSM−5	H_2O/ Toluene	180	14.1	0.436	5	0[a]	190	82.4[a]	N.d.	3
	MCM-Nb16	H_2O/ Toluene	100	3.19	0.383	3	6	170	59.9	N.d.	4
	eHTiNbO$_5$–MgO	H_2O/ Toluene	240	2.91	0.133	3	15	160	55.0	N.d.	5
	H-AM11	H_2O/ Toluene	360	3.19	0.049	3	0	160	54.0	N.d.	6
	Nb_2O_5	H_2O/ Toluene	90	3.19	0.640	-	-	170	50.0	N.d.	7
Monophasic Catalyst	NBO	H_2O/ CPME	240	10.0	0.218	3	0	180	68.0	N.d.	8
	$NbOPO_3$	H_2O	180	1.0	0.211	4	13	180	55.0	N.d.	9
	SAPO−34	H_2O/GVL	360	1.0	0.073	5	5	190	40.0	N.d.	10
	Nb_2O_5	H_2O	360	2.0	0.246	-	-	160	46.1	N.d.	11
	$W_{0.20}Nb_{0.80}O_x$	H_2O/EtOH	60	9.1	0.683	3	5	160	41.4	76	***This work***

N.d.: Not-determined.
[a] It has not been specified how the total furfural formed has been determined.

to be a robust and efficient acid catalyst for the furfural synthesis from xylose (C5 sugar) in monophasic solvent system under moderate reaction conditions, with furfural productivity higher than that achieved by other solid acid catalysts in both biphasic and monophasic systems. Of course, furfural yield reached with our W-Nb-O catalyst could be further improved, and future research will focus on two main strategies: i) the enhancement of the acidity of the systems by incorporating an additional element in the W-Nb-O Bronze structure, and ii) the evaluation of the catalytic system in a continuous flow fix-bed catalytic reaction system aiming to reduce the amount of humins formed during the process.

4. Conclusions

A series of solid acid catalysts based on W-Nb-O mixed oxides with either hexagonal or pseudo-crystalline Bronze-type structure have been synthesized through a hydrothermal method at moderate temperatures. It has been found that chemical composition of W-Nb-O materials is essential to tune textural and mainly acidic properties. Thus, best catalytic results for the dehydration of xylose to furfural were achieved for $\mathbf{W_{0.20}Nb_{0.80}O_x}$ catalyst, with a furfural selectivity comparable to that of homogeneous sulfuric acid under our optimal reaction conditions, which is the catalyst employed at industrial level. This achievement is attributed to the adequate combination of both Brønsted and Lewis acid sites given by the optimal W/Nb composition in the material, as well as to the low surface density of acidic sites that has been shown to be necessary for a smooth sugar dehydration this way reducing the non-desired formation of consecutive condensation products, mainly humins. Furthermore, this catalyst has demonstrated its activity and selectivity even after three consecutive catalytic cycles by maintaining unaltered its structure and chemical composition, thus becoming a robust and efficient catalyst for C5 sugars dehydration in aqueous media under moderate reaction conditions. Main results achieved for this optimal W-Nb-O catalyst in terms of stability and recyclability, carbon balances in reactions, and furfural productivity (calculated as $g_{Fur} \cdot g_{Cat}^{-1} \cdot h^{-1}$) were compared to these data reported or calculated for most relevant and recently reported solid acid catalysts, thus demonstrating that the W-Nb-O material is a competitive, robust and recyclable solid acid catalyst for the furfural production from C5 sugars. Moreover, this very good catalytic behavior makes this material suitable for upscaling furfural production from C5 sugars, a key step for this bio-derived platform molecule becoming more available for further applications [45], thus favoring the development of new strategies for obtaining renewable products, as for example the novel synthetic route for sustainable aviation fuels (SAFs) production starting from furfural very recently promoted by the HIGFLY (HIGee to Furanic-based jet Fuel technology, GA 101006618) European project [73].

CRediT authorship contribution statement

Agustín de Arriba: Writing – review & editing, Formal analysis, Investigation, Writing – original draft, Data curation. **Jesús López-Sánchez:** Formal analysis, Writing – original draft, Writing – review & editing, Investigation, Data curation. **López-Nieto José Manuel:** Validation, Funding acquisition, Data curation, Writing – review & editing, Resources, Investigation, Formal analysis, Conceptualization, Writing – original draft, Methodology. **Marcelo E. Domine:** Writing – review & editing, Investigation, Conceptualization, Writing – original draft, Supervision, Methodology, Funding acquisition, Validation, Resources, Formal analysis. **Francisco Cernicharo-Toledo:** Writing – review & editing, Investigation, Writing – original draft, Formal analysis, Data curation.

Declaration of Competing Interest

The authors declare that they have no known competing financial interests or personal relationships that could have appeared to influence the work reported in this paper.

Acknowledgements

Authors thank financial support by the Spanish Government (PID2021–125897OB-I00, PID2021–126235OB-C31, and PID2023–151036OA-I00) funded by MCIN/AEI/10.13039/501100011033 and FEDER funds. Financial support by European Commission, H2020 Program (HIGFLY Project, grant agreement N°101006618) is gratefully acknowledged. J.L.-S. acknowledges grant RYC2022–035912-I funded by MCIU/AEI/10.13039/501100011033 and by the European Social Fund Plus (ESF+). Authors also thank Miriam Parreño-Romero and the Electron Microscopy Service of Universitat Politècnica de València for their support.

Appendix A. Supporting information

Supplementary data associated with this article can be found in the online version at doi:10.1016/j.apcata.2025.120467.

Data Availability

Data will be made available on request.

References

[1] A. Demirbaş, Energy Convers. Manag. 42 (2001) 1357–1378, https://doi.org/10.1016/S0196-8904(00)00137-0.
[2] D.L. Klass, Encyclopedia of Energy, Elsevier Sci, London, 2004.
[3] D.L. Klass, Biomass for Renewable Energy, Fuels, and Chemicals, Press, A., Ed.; San Diego, 1998.
[4] A.C. Hansen, C.E. Goering, A.S. Ramadhas, Ethanol. Alternative Fuels Transportation, 1st Ed., e-book, CRC Press, 2011, pp. 129–166.
[5] C.E. Wyman, Appl. Biochem. Biotechnol. 45-46 (1994) 897–915, https://doi.org/10.1007/BF02941858.
[6] L.R. Lynd, J.H. Cushman, R.J. Nichols, C.E. Wyman, Science 251 (1991) 1318–1323, https://doi.org/10.1126/science.251.4999.1318.
[7] J. Baruah, B.K. Nath, R. Sharma, S. Kumar, R.C. Deka, D.C. Baruah, E. Kalita, Front. Energy Res. 6 (2018) 1–19, https://doi.org/10.3389/fenrg.2018.00141.
[8] A. Corma, S. Iborra, A. Velty, Chem. Rev. 107 (2007) 2411–2502, https://doi.org/10.1021/cr050989d.
[9] S. Sitthisa, W. An, D.E. Resasco, J. Catal. 284 (2011) 90–101, https://doi.org/10.1016/j.jcat.2011.09.005.
[10] B.H. Wojcik, Ind. Eng. Chem. 40 (1948) 210–216, https://doi.org/10.1021/ie50458a007.
[11] N. Merat, C. Godawa, A. Gaset, J. Chem. Technol. Biotechnol. 48 (1990) 145–159, https://doi.org/10.1002/jctb.280480205.
[12] O.W. Cass, Ind. Eng. Chem. 40 (1948) 216–219, https://doi.org/10.1021/ie50458a008.
[13] H.J. Brownlee, C.S. Miner, Ind. Eng. Chem. 40 (1948) 201–204, https://doi.org/10.1021/ie50458a005.
[14] C.D. Hurd, J.W. Garrett, E.N. Osborne, J. Am. Chem. Soc. 55 (1933) 1082–1084, https://doi.org/10.1021/ja01330a032.
[15] C. Rong, X. Ding, Y. Zhu, Y. Li, L. Wang, Y. Qu, X. Ma, Z. Wang, Carbohydr. Res. 350 (2012) 77–80, https://doi.org/10.1016/j.carres.2011.11.023.
[16] R. Weingarten, J. Cho, W.C. Conner, G.W. Huber, Green. Chem. 12 (2010) 1423–1429, https://doi.org/10.1039/C003459B.
[17] O. Sato, N. Mimura, Y. Masuda, M. Shirai, A. Yamaguchi, J. Supercrit. Fluids 144 (2019) 14–18, https://doi.org/10.1016/j.supflu.2018.10.004.
[18] A. Mandalika, T. Runge, Green. Chem. 14 (2012) 3175–3184, https://doi.org/10.1039/C2GC35759C.
[19] J. Köchermann, M. Klemm, Ind. Eng. Chem. Res. 62 (2023) 6886–6896, https://doi.org/10.1021/acs.iecr.3c00259.
[20] V. Krzelij, J. van Kampen, J. van der Schaaf, M.F. Neira d'Angelo, Ind. Eng. Chem. Res. 58 (35) (2019) 16126–16137, https://doi.org/10.1021/acs.iecr.9b00445.
[21] M. Papaioannou, R. Kleijwegt, J. van der Schaaf, M.F. Neira d'Angelo, Ind. Eng. Chem. Res. 58 (35) (2019) 16106–16115, https://doi.org/10.1021/acs.iecr.9b00604.
[22] W. Guo, H.C. Bruining, H.J. Heeres, J. Yue, AIChE J. 68 (5) (2022) e17606, https://doi.org/10.1002/aic.17606.
[23] A. Corma, Chem. Rev. 95 (1995) 559–614, https://doi.org/10.1021/cr00035a006.
[24] J.H. Clark, Acc. Chem. Res. 35 (2002) 791–797, https://doi.org/10.1021/ar010072a.
[25] T. Okuhara, Chem. Rev. 102 (2002) 3641–3666, https://doi.org/10.1021/cr0103569.
[26] I. Agirrezabal-Telleria, A. Larreategui, J. Requies, M.B. Güemez, P.L. Arias, Bioresour. Technol. 102 (2011) 7478–7485, https://doi.org/10.1016/j.biortech.2011.05.015.

[27] S.J. You, Y.T. Kim, E.D. Park, React. Kinet. Mech. Catal. 111 (2014) 521–534, https://doi.org/10.1007/s11144-013-0655-1.
[28] H. Chen, L. Qin, B. Yu, Biomass. Bioenergy 73 (2015) 77–83, https://doi.org/10.1016/j.biombioe.2014.12.013.
[29] P. Bhaumik, P.L. Dhepe, ACS Catal. 3 (2013) 2299–2303, https://doi.org/10.1021/cs400495j.
[30] C. García-Sancho, J.M. Rubio-Caballero, J.M. Mérida-Robles, R. Moreno-Tost, J. Santamaría-González, P. Maireles-Torres, Catal. Today 234 (2014) 119–124, https://doi.org/10.1016/j.cattod.2014.02.012.
[31] A.S. Dias, S. Lima, D. Carriazo, V. Rives, M. Pillinger, A.A. Valente, J. Catal. 244 (2) (2006) 230–237, https://doi.org/10.1016/j.jcat.2006.09.010.
[32] A.S. Dias, M. Pillinger, A.A. Valente, Appl. Catal. A Gen. 285 (2005) 126–131, https://doi.org/10.1016/j.apcata.2005.02.016.
[33] Y. Wang, F. Delbecq, W. Kwapinski, C. Len, Mol. Catal. 438 (2017) 167–172, https://doi.org/10.1016/j.mcat.2017.05.031.
[34] S.M. Bruce, Z. Zong, A. Chatzidimitriou, L.E. Avci, J.Q. Bond, M.A. Carreon, S. G. Wettstein, J. Mol. Catal. A Chem 422 (2016) 18–22, https://doi.org/10.1016/j.molcata.2016.02.025.
[35] H. Gao, H. Liu, B. Pang, G. Yu, J. Du, Y. Zhang, H. Wang, X. Mu, Bioresour. Technol. 172 (2014) 453–456, https://doi.org/10.1016/j.biortech.2014.09.026.
[36] C. García-Sancho, L. Sádaba, R. Moreno-Tost, J. Mérida-Robles, J. Santamaría-González, M. López-Granados, P. Maireles-Torres, ChemSusChem 6 (4) (2013) 635–642, https://doi.org/10.1002/cssc.201200881.
[37] A.S. Dias, S. Lima, P. Brandão, M. Pillinger, J. Rocha, A.A. Valente, Catal. Lett. 108 (2006) 179–186, https://doi.org/10.1007/s10562-006-0046-6.
[38] M.J.C. Molina, M.L. Granados, A. Gervasini, P. Carniti, Catal. Today 254 (2015) 90–98, https://doi.org/10.1016/j.cattod.2015.01.018.
[39] D.T. Win, Furfural-Gold from Garbage, Au J. Technol. 8 (2005) 185–190.
[40] K.J. Zeitsch, The Chemistry and Technology of Furfural and Its Many By-Products, 1st Ed., 13, Elsevier Sci, Amsterdam, 2000.
[41] W. De Jong, G. Marcotullio, Int. J. Chem. React. Eng. 8 (2010) A69, https://doi.org/10.2202/1542-6580.2174.
[42] D. Delgado, A. Fernández-Arroyo, M.E. Domine, E. García-González, J.M. López Nieto, Catal. Sci. Technol. 9 (2019) 3126–3136, https://doi.org/10.1039/C9CY00367C.
[43] M.E. Domine, J.M. López Nieto, D. Delgado Muñoz, A. Fernández-Arroyo, WO 2017162900 (2017).
[44] A. Abdullahi, K. Okumura, Mol. Catal. 570 (2025) 114669, https://doi.org/10.1016/j.mcat.2024.114669.
[45] J.P. Lange, Catal. Today 435 (2024) 114726, https://doi.org/10.1016/j.cattod.2024.114726.
[46] A. Jouve, S. Cattaneo, D. Delgado, N. Scotti, C. Evangelisti, J.M.L. Nieto, L. Prati, Appl. Sci. 9 (11) (2019) 2287–2301, https://doi.org/10.3390/app9112287.
[47] J. López-Sánchez, E. Navarro, A. Serrano, C. Granados-Miralles, A. del Campo, A. Quesada, P. Marín, ACS Appl. Electron. Mater. 2 (2020) 1484–1496, https://doi.org/10.1021/acsaelm.0c00252.
[48] Z. Gu, T. Zhai, B. Gao, X. Sheng, Y. Wang, H. Fu, Y. Ma, J. Yao, J. Phys. Chem. B 110 (47) (2006) 23829–23836, https://doi.org/10.1021/jp065170y.
[49] T. Fuchigami, K.I. Kakimoto, J. Mater. Res. 32 (2017) 3326–3332, https://doi.org/10.1557/jmr.2017.200.
[50] A. Chieregato, F. Basile, P. Concepción, S. Guidetti, G. Liosi, M.D. Soriano, C. Trevisanut, F. Cavani, J.M.L. Nieto, Catal. Today 197 (2012) 58–65, https://doi.org/10.1016/j.cattod.2012.06.024.
[51] D. Delgado, P. Concepción, A. Trunschke, J.M. López Nieto, Dalton Trans. 49 (2020) 13282–13293, https://doi.org/10.1039/D0DT02058C.
[52] J.M. Gallardo-Amores, V. Sánchez-Escribano, G. Ramis, G. Busca, Appl. Catal. B. Environ. 13 (1997) 45–56.
[53] D. Delgado, A. Fernández-Arroyo, N.La Salvia, M.E. Domine, J.M.L. Nieto, Chin. J. Catal. 40 (2019) 1778–1787, https://doi.org/10.1016/S1872-2067(19)63419-4.
[54] K. Omata, S. Izumi, T. Murayama, W. Ueda, Catal. Today 201 (2013) 7–11, https://doi.org/10.1016/j.cattod.2012.06.004.
[55] M.D. Soriano, P. Concepción, J.M.L. Nieto, F. Cavani, S. Guidetti, C. Trevisanut, Green. Chem. 13 (2011) 2954–2962, https://doi.org/10.1039/C1GC15622E.
[56] I.M. Szilágyi, J. Madarász, G. Pokol, P. Király, G. Tárkányi, S. Saukko, J. Mizsei, A. L. Tóth, A. Szabó, K. Varga-Josepovits, Chem. Mater. 20 (2008) 4116–4125, https://doi.org/10.1021/cm800668x.
[57] S.J. Hug, D. Bahnemann, J. Electron Spectros. Relat. Phenom. 150 (2006) 208–219, https://doi.org/10.1016/j.elspec.2005.05.006.
[58] J. López-Sánchez, A. Serrano, A. del Campo, A. Muñoz-Noval, E. Salas-Colera, M. Cabero, M. Varela, M. Abuín, G.R. Castro, J. Rubio-Zuazo, O. Rodríguez de la Fuente, N. Carmona, J. Alloy. Compd. 892 (2022) 162061, https://doi.org/10.1016/j.jallcom.2021.162061.
[59] W. Song, R. Zhang, X. Bai, Q. Jia, H. Ji, J. Mater. Sci. Mater. Electron 31 (2020) 610–620, https://doi.org/10.1007/s10854-019-02565-6.
[60] L. Wang, H. Zhang, Y. Yin, Y.L. Zhou, X. Yin, T. Wang, J. Zeng, W. Wang, W. Zhou, D. Tang, J. Phys. D. Appl. Phys. 56 (2023) 185501–185511, https://doi.org/10.1088/1361-6463/acbc87.
[61] A. Ihyadn, A. Lahmar, D. Mezzane, L. Bih, A. Alimoussa, M. Amjoud, M.E. Marssi, I. ALuk'yanchuk, Mater. Res. Express 6 (2019) 115203, https://doi.org/10.1088/2053-1591/ab4569.
[62] A. Senapati, S.K. Barik, R. Venkata Krishnan, S. Chakraborty, H. Jena, J. Therm. Anal. Calor. 148 (2023) 355–369, https://doi.org/10.1007/s10973-022-11760-3.
[63] J.M. Jehng, I.E. Wachs, Chem. Mater. 3 (1) (1991) 100–107, https://doi.org/10.1021/cm00013a025.
[64] Y. Wang, S. Aghamohammadi, D. Li, K. Li, R. Farrauto, Appl. Catal. B Environ. 244 (2019) 438–447, https://doi.org/10.1016/j.apcatb.2018.11.066.
[65] M. Grundner, J. Halbritter, J. Appl. Phys. 51 (1980) 397–405, https://doi.org/10.1063/1.327386.
[66] T.H. Kim, H.J. Ryu, K.K. Oh, Bioresour. Technol. 218 (2016) 367–372, https://doi.org/10.1016/j.biortech.2016.06.106.
[67] M.D. Víctor-Ortega, J.M. Ochando-Pulido, A. Martínez-Ferez, Sep. Purif. Technol. 173 (2017) 1–8, https://doi.org/10.1016/j.seppur.2016.08.037.
[68] J. Iglesias, J.A. Melero, G. Morales, M. Paniagua, B. Hernández, ChemCatChem 8 (2016) 2089–2099, https://doi.org/10.1002/cctc.201600292.
[69] O. Ershova, J. Kanervo, S. Hellsten, H. Sixta, The role of xylulose as an intermediate in xylose conversion to furfural: insights via experiments and kinetic modelling, RSC Adv. 5 (82) (2015) 66727–66737, https://doi.org/10.1039/c5ra10855a.
[70] L. Vanoye, M. Fanselow, J.D. Holbrey, M.P. Atkins, K.R. Seddon, Green. Chem. 11 (2009), https://doi.org/10.1039/B817882H, 390–39.
[71] C. Fang, W. Wu, H. Li, T. Yang, W. Zhao, Z. Wang, S. Yang, Energy Sources Part A Recover. Util. Environ. Eff. 39 (21) (2017) 2072–2077, https://doi.org/10.1080/15567036.2017.1402103.
[72] L.F. Lima, J.L.M. Lima, D.S.S. Jorqueira, R. Landers, S.F. Moya, R.S. Suppino, React. Kinet. Mech. Catal. 132 (2021) 73–92, https://doi.org/10.1007/s11144-021-01931-y.
[73] HIGFLY European Project: HIGee to Furanic-based jet Fuel technology (GA 101006618). ⟨https://www.higfly.eu/⟩, 2025 (Accessed 28 march, 2025).